

Combined visible and infrared Thomson scattering on the MAST experiment

M. J. Walsh, E. R. Arends, P. G. Carolan, M. R. Dunstan, M. J. Forrest et al.

Citation: *Rev. Sci. Instrum.* **74**, 1663 (2003); doi: 10.1063/1.1537882

View online: <http://dx.doi.org/10.1063/1.1537882>

View Table of Contents: <http://rsi.aip.org/resource/1/RSINAK/v74/i3>

Published by the [American Institute of Physics](#).

Related Articles

Study of the plasma wave excited by intense femtosecond laser pulses in a dielectric capillary
[Phys. Plasmas](#) **19**, 093121 (2012)

Note: Statistical errors estimation for Thomson scattering diagnostics
[Rev. Sci. Instrum.](#) **83**, 096106 (2012)

Imaging spectroscopy diagnosis of internal electron temperature and density distributions of plasma cloud surrounding hydrogen pellet in the Large Helical Device
[Rev. Sci. Instrum.](#) **83**, 093506 (2012)

Temporally resolved characterization of shock-heated foam target with Al absorption spectroscopy for fast electron transport study
[Phys. Plasmas](#) **19**, 092705 (2012)

Synchronized operation by field programmable gate array based signal controller for the Thomson scattering diagnostic system in KSTAR
[Rev. Sci. Instrum.](#) **83**, 093505 (2012)

Additional information on *Rev. Sci. Instrum.*

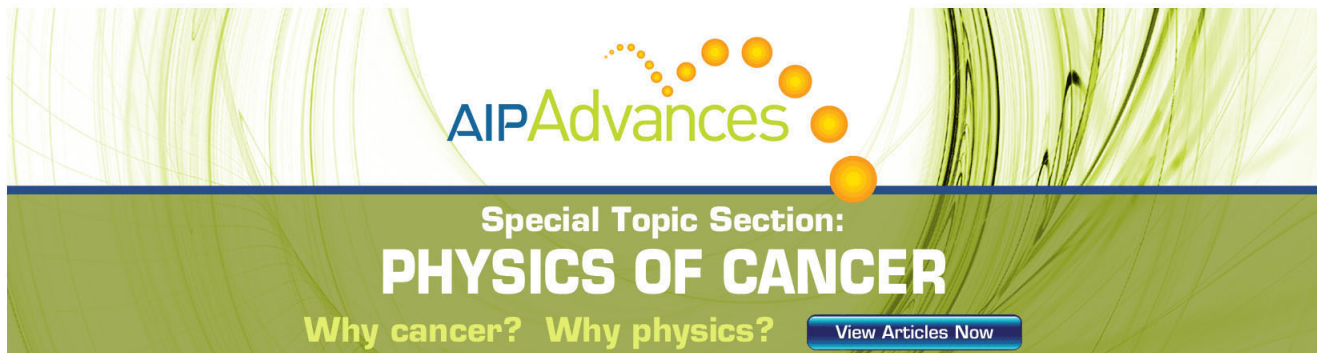
Journal Homepage: <http://rsi.aip.org>

Journal Information: http://rsi.aip.org/about/about_the_journal

Top downloads: http://rsi.aip.org/features/most_downloaded

Information for Authors: <http://rsi.aip.org/authors>

ADVERTISEMENT



AIP Advances

Special Topic Section:
PHYSICS OF CANCER

Why cancer? Why physics? [View Articles Now](#)

Combined visible and infrared Thomson scattering on the MAST experiment

M. J. Walsh,^{a)} E. R. Arends,^{b)} P. G. Carolan, M. R. Dunstan, M. J. Forrest, S. K. Nielsen,^{c)} and R. O’Gorman^{d)}
EURATOM/UKAEA Fusion Association, Culham Science Centre, Abingdon, Oxfordshire OX14 3DB, United Kingdom

(Presented on 8 July 2002)

A dual laser Thomson scattering system is implemented in the Mega Amp Spherical Tokamak (MAST). The complementary features of each approach are exploited. One system is ideally suited to measuring detailed profile behavior across the plasma while the other is ideally suited though not exclusively to studying fast changing events and general characterization of the plasma. Both systems are designed to be flexible and allow future expansion to suit the needs of a changing physics program. © 2003 American Institute of Physics. [DOI: 10.1063/1.1537882]

I. INTRODUCTION

Many physics campaigns on present tokamak experiments require detailed spatial and temporal measurements for investigating the dynamics of transport barriers, ELM’s, and sawteeth as well as the structures associated with magnetic islands and the variations associated with plasma evolution and transport.¹ These requirements place high demands on a Thomson scattering (TS) system that monitors the behavior of the electron temperature and density profiles. Current technology suitable for TS, in the visible, using ruby lasers, excels in high definition spatial measurements while Nd:YAG lasers, in the infrared, facilitate multi-time probing. The advantages of both systems are exploited in the Mega Amp Spherical Tokamak (MAST). This TS system is designed to provide very high spatial resolution using a ruby laser and charge coupled device (CCD) system, as well as high temporal sampling using Nd:YAG lasers and a compact polychromator approach.

A 300 point single pulse ruby laser TS system² produces full diameter profile measurements of T_e and n_e , providing, for example, detailed profile characterization of very steep H -mode edge pedestals. This system is enhanced by a modular TS assembly that has a 100 Hz (2×50) Nd:YAG 20 point system that is quasioxial with the ruby laser beam and uses much of the same input and collection optics and both systems avail of a common laser dump. This system is easily expandable to more lasers and more spatial points. Future enhancements will be tailored to the physics program demands, while simultaneously maintaining diagnostic availability. In order to implement the aforementioned scheme, common components are identified to minimize machine area and viewing port usage.

^{a)}Also at: Walsh Scientific Limited, Culham Science Centre, Abingdon, Oxfordshire OX14 3EB, UK; electronic mail: michael.walsh@ukaea.org.uk

^{b)}Also at: FOM Institute for Plasma Physics “Rijnhuizen”, P.O. Box 1207, 3430 BE Nieuwegein, Netherlands.

^{c)}Also at: Institut for Fysik og Astronomi, Aarhus Universitet, Ny Munkegade, DK-8000, Denmark.

^{d)}University College Cork, Cork, Ireland.

II. COMMON OPTICS

The common components in this system are the laser flight lines, the collection lens; and the laser dump. The lasers are arranged, as in Fig. 1, to be colinear and use a common flight line with different apertures to control the stray light, particularly at the central stack area. The ruby and Nd:YAG beams are focused using separate 4 m planoconvex lenses toward the plasma center but avoiding the central stack (by ~ 45 mm) and the beams are arranged to be slightly smaller than the image of the fiber bundles at the plasma periphery. These beams lie $+15.5$ mm above and -14.5 mm below the machine central midplane for the Nd:YAG and ruby lasers, respectively, and this distance is small compared to a typical plasma vertical extent of over 2 m. This arrangement allows the image of the fiber bundles to be separated in the image plane of the collection lens. The lens has a magnification of ~ 0.15 allowing sufficient space to mount fiber bundles for both laser systems in a straightforward fashion. The design lends itself to modular upgrades such as more spatial channels.

The ruby system image plane has 26 slots to insert fiber bundles and the arrangement allows complete and continuous viewing of the scattered light across the plasma. The Nd:YAG image-plane arrangement has 27 slots which are designed to allow the adjacent fiber bundles to be completely butted together. In particular, each slot can take two specially made fiber bundles giving a total of 54 possible spatial positions in the present configuration. Initially, this will be occupied by 21 fiber bundles whose positions satisfy the current physics requirements. The bundles are made from APC210/230 fiber with a common bundle height of 0.82 mm, giving a bundle height of ~ 5.5 mm in the plasma for both systems.

The collection lens is designed to collect the scattered light across the full field of view of the lens while providing a light cone of $f/1.75$ on to each fiber bundle. At this f number more than 60% of the light (including fill factor losses, etc.) is transmitted over fiber bundle lengths of the order of 20 m to 40 m. The light is collected from the plasma at $f/12$

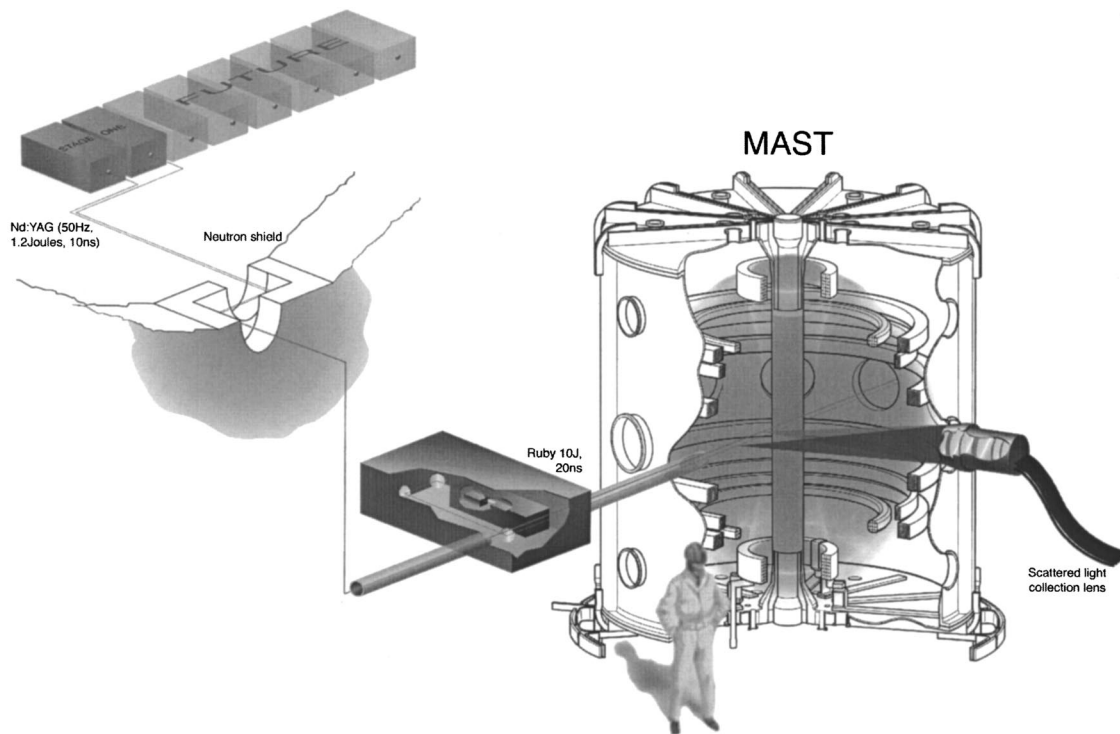


FIG. 1. Schematic of the MAST vessel showing the arrangement of the lasers and the light collection systems.

for the Nd:YAG system while the aperture is slightly reduced to $f/14.9$ for the ruby system due to limitations set by the grating spectrometer. This is partially compensated for by the use of a large grating area. Even though this lens was originally designed for a ruby laser, ray tracing analysis shows that the imaging performance remains as for the ruby system up to the Nd:YAG wavelength of 1064 nm while measurements show that the transmission varies by less than 20% over the large wavelength range.

The laser light is coupled into the plasma via a single large Brewster angle window. This allows both laser beams to be transmitted very efficiently without the need for special coatings while simultaneously reducing the risk of damaging the laser window due to the angle-increased surface area. The beams are finally absorbed by a laser dump that is located close to the machine vessel wall. A graphite laser dump

is used which can tolerate the high-power densities placed upon it. The dump can be retracted from the laser beam path to allow special beam tests and alignment of the whole system. The alignment is maintained using HeNe lasers arranged to be coaxial with the high-power lasers and drop-in targets that act as reference markers.

III. HIGH SPATIAL RESOLUTION RUBY SYSTEM

A low divergence, 10J Q -switched ruby laser source and a custom designed light dispersion system are employed³ to realize high spatial resolution (~ 300 points sampled). The light is imaged onto the dispersion system via a quasicontinuous array of fiber optic bundles (at $f/2.24$). A gated (GaAs) image intensifier is used as an optical shutter to allow only the scattered light period (30–40 ns) through to the CCD detector. A wavelength range of 550 nm to ~ 900 nm is allowable although presently this is limited by the image intensifier from ~ 580 to ~ 900 nm. The system is designed to measure temperatures between 25 and 4 keV and densities above $3 \times 10^{18} \text{ m}^{-3}$ with high spatial accuracy, or alternatively there is the flexibility of integrating the spatial data (at pixel level) to provide more signal at the expense of less spatial channels. Furthermore, the spectrometer slit width can be profiled in width to increase the potential dynamic range of the system, e.g., to match the plasma edge, to allow much lower electron temperatures to be measured if necessary.

The light is collected across a 1.5 m plasma length and mapped onto ~ 300 pixels on the CCD camera. The fiber bundles are arranged so that the spatial resolution is maintained in the mapping. The spatial resolution of the system can be seen from Fig. 2, where the normalized magnetic flux

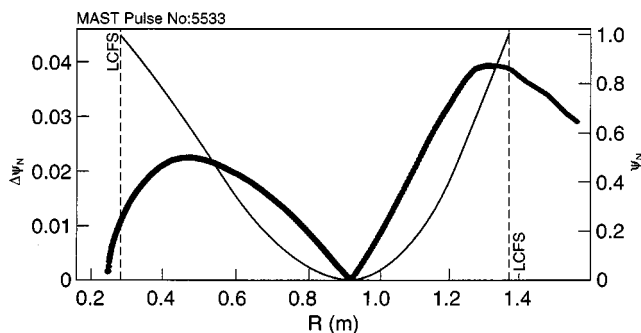


FIG. 2. NFR or $\Delta R \cdot \partial \psi_N / \partial R$ of the ruby system plotted as a function of major radius. This shows the measuring power of the system at each position in space. It is clear from this graph that the best performance of this system is at the inboard radius where $\Delta \psi_N$ goes below 0.005. The normalized flux, $\psi_N = (\psi_0 - \psi) / (\psi_0 - \psi_{\text{edge}})$ is also shown along with the last closed flux surface.

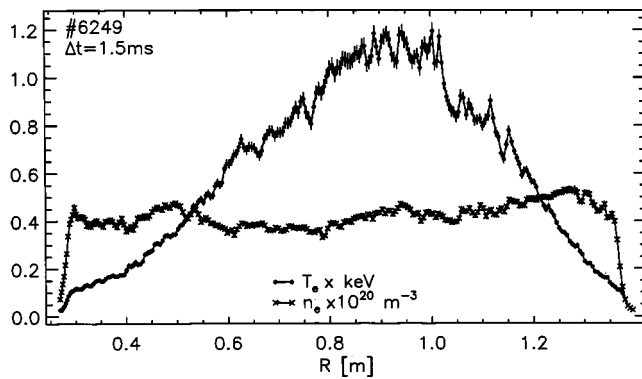


FIG. 3. Detailed electron temperature and density profiles from the 300 point ruby laser TS system showing full diameter profile measurements. These profiles are taken 1.5 ms after ELM event.

resolution (NFR) or $\Delta\psi_N = \Delta R \cdot \partial\psi_N / \partial R$ is plotted as a function of major radius. This shows the resolving power of the system at each position in space. It is clear from this graph in Fig. 2 that the best performance of this system is at the inboard radius where $\Delta\psi_N$ goes below 0.005. The highest resolution is at the inner edge due to tangency of the laser beam with the flux surfaces and the high resolution in the core is due to the slowly changing flux field. This inner edge resolution is ultimately limited by the beam diameter, which is approximately 2–3 mm at this point. The normalized flux, ψ_N , is defined as $\psi_N = (\psi_0 - \psi) / (\psi_0 - \psi_{\text{edge}})$.

Figure 3 shows the results from the 300 point ruby laser TS system producing full diameter profile measurements of T_e and n_e . The discharge shown in Fig. 3 give examples of the high spatial resolution especially at the edge where detailed profile characterization of *H*-mode pedestals is observed.^{4,5}

IV. Nd:YAG SYSTEM

To achieve the physics objectives of the MAST programme, it was decided that a multilaser approach was appropriate. A number of Nd:YAG lasers which can each produce 50 pulses/s at 1.2 J of energy are utilized. The design allows for up to eight lasers, although initially only two are installed. The triggering arrangement permits multiple lasers to be triggered simultaneously for total higher energy; alternatively, equispaced pulses can be used for normal operation or the pulses can be grouped to produce a “burst mode” of pulses that are repeated at 50 Hz. The time separation in the latter mode can be down to around 100 ns if necessary.

To accommodate eight lasers in the design, the first four lasers will be arranged to be close together in the horizontal plane and focused to cross over at the plasma center. The other four lasers will be accommodated by using an optical switching technique that will make them coaxial with the first four.

For optimum laser performance, a warm up time of the order of 2 min is required. This would put a very high heat load on the beam dump internal to the plasma vessel. This is avoided by having individual water cooled dumps on each laser. Then, during the laser warm-up time, the laser power is

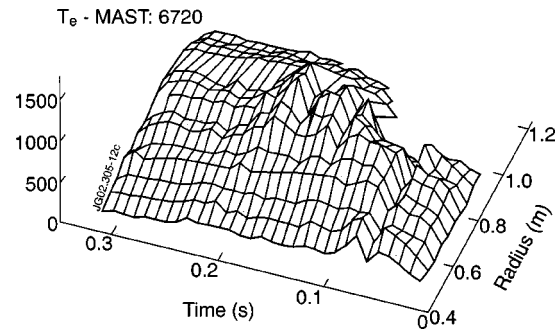


FIG. 4. Surface plot of electron temperature data from 100 Hz Nd:YAG laser system. The effect of sawteeth and other MHD events can clearly be seen in the time development of the discharge.

confined to the individual lasers and only allowed through to the final laser dump in the vessel during the plasma shot period. The scattered light is relayed to compact polychromators via fiber bundles. The maximum light input is given by the maximum fiber bundle diameter of 3 mm and the number of 1.75. The fiber bundle holder has appropriate mechanical adjustment and is easily removable/insertable with kinematic localization. The device is designed to have seven spectral channels and presently five channels are occupied in each polychromator. Raman scattering using N_2 is used for density calibration. In the present setup, these devices are able to measure from a few eV to approximately 20 keV. Temperature stabilization of the avalanche photodetectors is achieved electronically.

A optical-duplexing technique is used to increase the number of spatial channels observed. To achieve this, half of the fibers in the fiber bundle are extended to create a time delay of about 100 ns. This means that a spectrometer can measure two spatial channels at once. At present, we have 20 spatial channels and 14 spectrometers of which 6 are duplexed. The duplexed fiber bundles are 4.2 mm wide and the nonduplexed fiber bundles are 6 mm wide, and when imaged to the plasma give a scattering length of 25 mm and 40 mm, respectively. This corresponds to a radial resolution of the order of 2–3 mm at the inner plasma edge.

The scattered pulses are sampled using 8 bit, 1 giga-sample/s analog-to-digital converters which can be further enhanced with the use of a signal delay technique. This collection technique allows analysis of the signals in different ways to maximize the data extracted. In particular, it allows the measurement of the background fluctuation level in the individual spectrometer channels due to the plasma light. This system is now operational and results are shown in Fig. 4.

ACKNOWLEDGMENTS

This work is funded by the U.K. Department of Trade and Industry and Euratom. The work carried out by the MAST team and especially S. Manhood and S. Shibaev is greatly appreciated. The authors are indebted to A. W. Morris, N. J. Lopes Cardozo, A. H. Sørensen, and S. L. Prunty for their support during the project.

¹A. Sykes *et al.*, Phys. Plasmas **8**, 2101 (2001).

²E. R. Arends, Ph.D. thesis, Technische Universiteit Eindhoven, The Netherlands, 2003.

³M. J. Walsh *et al.*, Rev. Sci. Instrum. **70**, 742 (1999).

⁴M. R. Tournianski *et al.*, Rev. Sci. Instrum. (these proceedings).

⁵E. R. Arends, M. J. Walsh, N. J. Lopes Cardozo *et al.*, Proceedings of the 28th European Physical Society Conference on Controlled Fusion and Plasma Physics, Madeira, June 2001, Vol. 25A, pp. 589–592.